ChemComm

COMMUNICATION

View Article Online
View Journal | View Issue

Cite this: *Chem. Commun.*, 2019, 55, 12308

Received 3rd September 2019,
Accepted 19th September 2019

DOI: 10.1039/c9cc06869d

rsc.li/chemcomm

In vivo ratiometric tracking of endogenous β-galactosidase activity using an activatable near-infrared fluorescent probe†

Limin Shi,‡ Chenxu Yan,‡ Yiyu Ma, Ting Wang, Zhiqian Guo * and Wei-Hong Zhu

Herein, we developed a dual-channel and light-up near-infrared fluorescent probe for ratiometric sensing of β-galactosidase (β-gal) activity. The well-designed probe, which shows ratiometric optical response with a significant red-shift (from 575 nm to 730 nm), was successfully applied to detect endogenous β-gal activity in SKOV-3 cells and tumor-bearing mice.

Abnormal tumor microenvironmental factors such as hypoxia,[1] low pH,[2] and overexpressed tumor-related enzymes[3–6] are widely accepted as the features of tumor tissue.[7] In particular, β-galactosidase (β-gal) is known as an important biomarker involved in tumorigenesis and metastasis of ovarian cancers. For example, high levels of β-gal activity were detected in several metastatic ovarian cancer cells (including SHIN3, SKOV3, *etc.*) compared with that in a non-transformed human cell line.[8] Thus, the assessment of endogenous β-gal activity *in vivo* is a commonly accepted method for clinical diagnosis and therapeutic evaluation of cancers.[9] Apparently, fluorescence imaging offers great potential for visualizing β-gal activity in preclinical diagnosis.[10–14] Although a number of responsive fluorescent probes have been reported for tracking β-gal,[15,16] the short emission extremely hinders their *in vivo* applications due to the limited tissue penetration depth and inevitable auto-fluorescence interference from biosystems.[17–20] In addition, the OFF–ON detecting pattern makes it difficult to precisely acquire β-gal expression in tumors, which is obstructive for evaluation of the cancer therapeutic efficacy.[21,22] Therefore, a ratiometric near-infrared (NIR) fluorescent probe for tracking endogenous β-gal is urgently required for *in vivo* accurate quantification analysis.[23–27]

4,4-Difluoro-4-bora-3*a*,4*a*-diaza-*s*-indacene (BODIPY) dyes have outstanding photophysical properties that make them good candidates for constructing fluorescent probes, such as high quantum yields, excellent photostability and chemical stability under physiological conditions.[28–30] Sparked by the new tactics in the functionalization of the 1,3-dimethyl-BODIPY core, due to its fine-tuned properties and easier purification procedures, a veritable BODIPY renaissance has come into being.[31] However, most of the current BODIPY-based probes focused on the OFF–ON response mode use the photon electron transfer (PET) mechanism.[32] In contrast, it would be an effective approach to construct ratiometric BODIPY probes by a typical intramolecular charge transfer (ICT) process.[33] In particular, when an electron-donating group (*e.g.* hydroxy) is covalently conjugated with the 1,3-dimethyl-BODIPY core, a remarkable shift in the emission spectra can be obtained with effective ICT properties, making it an ideal NIR ratiometric fluorescent reporter for *in vivo* application. Thus, we envision that a NIR ratiometric sensing of β-gal can be achieved by regulating the ICT process of a monostyryl-substituted BODIPY probe before and after the response with β-gal.

In this study, we report a NIR ratiometric probe (BODIPY-βgal) that can be used for accurately visualizing and analyzing the activity of β-gal *in vivo*. In our probe, monostyryl-substituted BODIPY (BODIPY-OH) is utilized as an NIR and wavelength-controllable chromophore, and a β-gal cleavable unit (β-galactopyranoside) as an enzyme-active trigger (Scheme 1). Upon reaction between the probe and β-gal, BODIPY-βgal is unmasked and converted into the deprotected product (BODIPY-OH in the phenolate form) in a physiological context. As expected, a colorimetric change in the absorption spectra and a remarkable red-shift to the NIR region in the emission spectra were observed. Herein, we focus on regulating the ICT process to achieve a ratiometric response which enables the direct and accurate monitoring of intracellular β-gal distribution in living cells and animals.

The general approach for the synthesis of β-gal probes involves a deacetyl step in a strong alkaline solution (by using NaOMe/MeOH) to attach the β-galactopyranoside group as an activatable unit.[34] However, owing to the poor chemical stability of BODIPY dyes in strong alkaline solution, it is extremely

State Key Laboratory of Bioreactor Engineering, Shanghai Key Laboratory of Functional Materials Chemistry, Institute of Fine Chemicals, School of Chemistry and Molecular Engineering, East China University of Science & Technology, Shanghai 200237, China. E-mail: guozq@ecust.edu.cn

† Electronic supplementary information (ESI) available: Experimental details and additional figures and table. See DOI: 10.1039/c9cc06869d

‡ These authors contributed equally to this work.

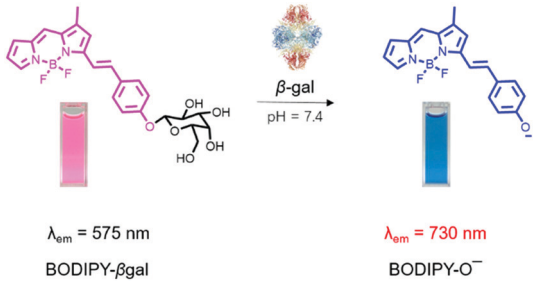

Scheme 1 Ratiometric tracking of endogenous β-gal activity using an activatable near-infrared probe BODIPY-βgal.

difficult to synthesize a BODIPY-based β-gal probe. In order to overcome the hurdles, we innovatively described an alternative synthetic route (Scheme 2): initially a de-protected key intermediate compound **2** was successfully synthesized, and then the target product BODIPY-βgal was effectively obtained *via* a typical Knoevenagel reaction within the neutral pH range.

To test the validity of our designed probe, the spectral properties of BODIPY-βgal were investigated with β-gal in an optimal physiological buffer solution. Upon titration with β-gal (5 U), the absorption peak sharply decreased at 560 nm, and a concomitant new absorption peak appeared at 620 nm (Fig. 1a), which is in perfect accordance with the absorption of BODIPY-O$^-$ (Fig. S1, ESI†). In addition, an obvious color change from pink to dark blue allows the colorimetric detection of β-gal using the naked eye, which is invoked by a red-shift of *ca.* 60 nm in the absorption spectra.

As expected, a clear bathochromic shift in the emission spectra was observed. Initially, BODIPY-βgal possessed a strong fluorescence signal at 575 nm (Table S1, ESI†), but a very weak fluorescence signal at 730 nm. In the presence of β-gal, there was a significant new enhanced emission peak at 730 nm upon excitation at 660 nm (Fig. 1c), whereas the initial fluorescence at 575 nm was decreased (Fig. 1b). These aforementioned observations demonstrated that upon a specific reaction of BODIPY-βgal with β-gal, there was a light-up NIR fluorescent signal with a significant red-shift (*ca.* 155 nm). Clearly, the distinct large red-shifted fluorescence response confirms that β-gal controlled hydrolysis liberates the oxygen atom of BODIPY-βgal as a strong electron donor, thereby shifting the emission maximum to the NIR region. In addition, the ratiometric fluorescent signal (I_{730nm}/I_{575nm}) depends

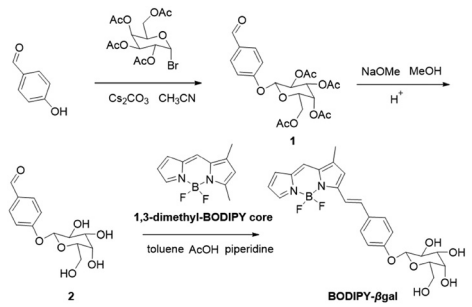

Scheme 2 Synthetic route of BODIPY-βgal.

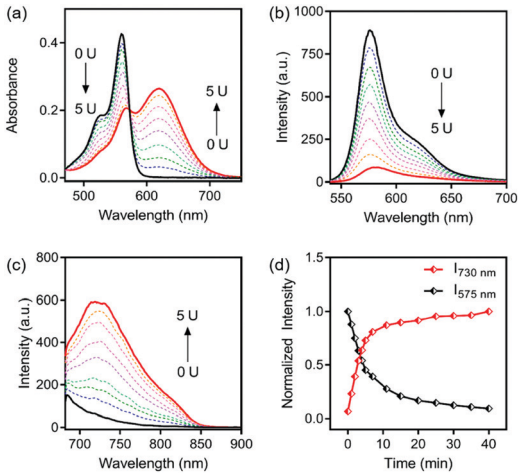

Fig. 1 Spectral profiles of BODIPY-βgal (10 μM) incubation with β-gal (5 U) in a mixture solution (phosphate-buffered saline (PBS)/dimethyl sulfoxide (DMSO) = 1 : 1 v : v, pH = 7.4). Absorption (a) and fluorescence spectra, λ_{ex} = 530 nm (b) and λ_{ex} = 660 nm (c); and (d) time-dependent fluorescence intensity I_{730nm} and I_{575nm}.

linearly as a function of the β-gal concentration (from 0 U to 3 U) at a fixed incubation time with a detection limit of 4.6×10^{-3} U mL^{-1} (Fig. S2 and S3, ESI†). Fig. 1d depicts the fluorescent ratio signal (I_{730nm} and I_{575nm}) as a function of time. Dual-channel fluorescent signal both take around 30 min to reach a plateau. We also evaluate the sensing performance of BODIPY-βgal in different pH solutions. Notably, BODIPY-βgal displayed similar dual-channel response in pH 6.0 (Fig. S4, ESI†), suggestive of its application in an acidic tumor microenvironment. Thus, these results offer a possibility to quantitatively and rapidly detect β-gal using the intensity ratios of I_{730nm}/I_{575nm}.

To further confirm that the leaving group could be specifically cleaved by β-gal and accompanied by *in situ* release of the fluorophore BODIPY-OH, HPLC and HRMS analyses were systemically performed. As shown in Fig. S5 (ESI†), the retention time of free BODIPY-βgal and BODIPY-OH is 4.0 and 6.7 min, respectively. After reaction with 5U β-gal, BODIPY-βgal exhibited an intense peak with a retention time of 6.7 min, suggesting that BODIPY-βgal is a substrate of β-gal and the sensing product is exclusively BODIPY-OH. Moreover, the cleavage product was further unambiguously confirmed by HRMS analysis. In the ensemble system of BODIPY-βgal and β-gal, the peaks of BODIPY-βgal and its cleavage product were found to be at *m*/*z* 485.18 and 323.16, respectively (Fig. S6, ESI†). Collectively, all of these results substantiate that the enzyme-catalyzed reaction *in situ* produces BODIPY-OH with NIR fluorescence.

We next investigated the photostability, pH stability and selectivity of probe BODIPY-βgal. Time-dependent photobleaching measurements show that BODIPY-OH still maintained 60% absorbance after sustained irradiation for 10 min, while the absorbance of ICG (an FDA approved NIR dye) as a control sharply decreased and reached a minimum level under the same irradiation conditions (Fig. S7, ESI†). These data demonstrate that the BODIPY-OH dye is more photostable than ICG. To gain insight into the influence of the hydroxyl group

and the β-galactopyranoside group in the BODIPY fluorophore, we examined the pH effect on the photophysical properties of BODIPY-OH and BODIPY-βgal. As the pH increased from 1.7 to 10.0, the emission peak of BODIPY-OH around 575 nm decreased significantly, while a new red-shifted emission band was observed around 730 nm (Fig. S8 and S9, ESI†). This large red-shift (155 nm) in the emission spectra with increased pH can be explained by the deprotonation of BODIPY-OH. Interestingly, the dual-channel emission of BODIPY-βgal shows stable photophysical properties in the pH range of 1.7–10.0 (Fig. S9, ESI†). These results show that the β-galactopyranoside group stabilizes the form of BODIPY-βgal but not that of BODIPY-OH. Besides, BODIPY-βgal also displayed excellent stability in fresh human serum (Fig. S10, ESI†). Furthermore, BODIPY-βgal showed excellent selectivity towards β-gal over other competitive bioanalytes because of the β-galactopyranoside unit as a specific enzyme-active trigger moiety, suggesting its potential as a bioprobe for tracking β-gal in living cells (Fig. S11, ESI†).

Encouraged by the desirable fluorescence response of BODIPY-βgal with β-gal, the probe for ratiometric tracking of endogenous β-gal activity was evaluated in living cells. Initially, the cytotoxicity of the probes was determined by MTT assay (Fig. S12, ESI†). The results indicated that the cell viability was still as high as 95% even after incubation with 20 μM BODIPY-βgal for 24 h, suggesting low cytotoxicity towards the cells. Based on the excellent biocompatibility, the dual-channel cell imaging was investigated by confocal laser scanning microscopy (CLSM). Herein, human ovarian cancer cells SKOV-3 were chosen as cell models because of their high levels of endogenous β-gal, whereas human hepatic cancer cells HepG2 as a contrast.

After incubating SKOV-3 with BODIPY-βgal (10 μM) for 30 min, we observed weak fluorescence in the green channel (570–620 nm) while significant NIR fluorescence in the red channel (670–800 nm) (Fig. 2a), indicating that β-gal is overexpressed in the cancer cells SKOV-3. To verify that the obtained fluorescence signal is indeed derived from endogenous β-gal activity, an inhibitor assay was performed (Fig. 2b). When SKOV-3 cells were exposed to 1 mM D-galactose (an inhibitor of β-gal) for 0.5 h and then treated with BODIPY-βgal for 0.5 h, the NIR fluorescence signal was clearly blocked, but a strong fluorescence from the green channel was observed, illustrating that these distinct signal changes were triggered by intracellular endogenous β-gal. In comparison, upon incubation with cancer cells HepG2, a bright fluorescence signal was observed in the green channel, whereas weak NIR fluorescence was observed in the red channel (Fig. 2c), suggesting that the intracellular β-gal activity in HepG2 cells is very low. Furthermore, the emission ratio value F_{red}/F_{green} of BODIPY-βgal in living cells was in accordance with the aforementioned dual-channel cell imaging (Fig. 2d). These results confirmed that BODIPY-βgal could react with endogenous β-gal and emit strong NIR fluorescence, which is consistent with the *in vitro* spectral experiments.

On the basis of the BODIPY-βgal optical properties and the above intracellular imaging of β-gal, we next examined its capability for real-time *in vivo* visualization of β-gal activity in tumors. Human lung xenograft tumor cells (A549 cells, without overexpressed β-gal) of the mice model were utilized. Living mice were pre-injected with β-gal to establish a mouse model with overexpressed β-gal at the tumor site and then injected orthotopically with BODIPY-βgal (Fig. 3c and d). On the other hand, the nude mice were pre-injected with PBS (and then injected with BODIPY-βgal) as a control (Fig. 3a and b). Notably, the control group displays a distinct fluorescence emission at the 600 nm channel, while a non-fluorescent signal at the 730 nm channel (Fig. 3a and b). In comparison, for the pre-treated-β-gal tumor-bearing mouse, after merely 5 min post-injection, the fluorescence signal at 730 nm was already clearly appreciated in tumor cells, indicative of the rapid activation of BODIPY-βgal with β-gal *in situ*. The NIR signal reached a

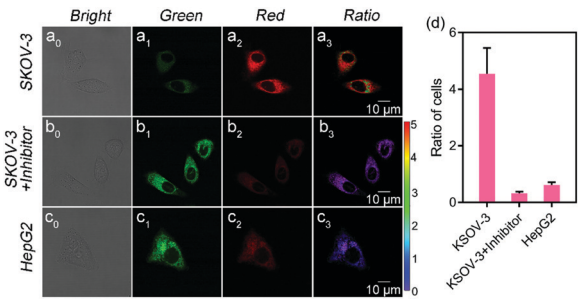

Fig. 2 CLSM images of SKOV-3 and HepG2 cells incubated with BODIPY-βgal (10 μM) for 0.5 h: (a) SKOV-3 cells and (b) SKOV-3 cells pretreated with 1 mM inhibitor for 0.5 h and (c) HepG2 cells. Note: the green channel obtained from 570 to 620 nm, λ_{ex} = 560 nm; the red channel obtained from 670 to 800 nm, λ_{ex} = 660 nm; ratiometric images generated from the red and green channel. (d) The emission ratio value F_{red}/F_{green} of BODIPY-βgal with β-gal in living cells in the absence and presence of the inhibitor. Error bars represent the standard deviation (S.D.) with n = 3.

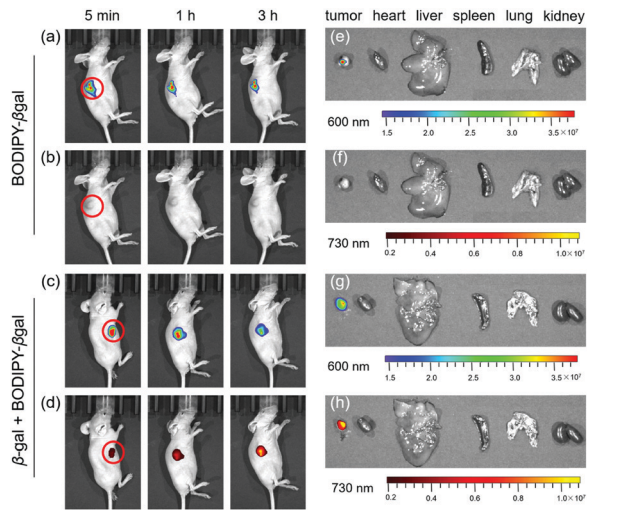

Fig. 3 Tumor-bearing mice were pre-treated with PBS (a, b, e and f) or β-gal at the tumor site (c, d, g and h) and then injected orthotopically with BODIPY-βgal (0.048 mg kg^{-1}). (a–d) *In vivo* dual-channel fluorescence imaging of the β-gal activity in xenograft tumor bearing mice at various times (5 min, 1 h and 3 h) after tumor injection. (e and f) *Ex vivo* fluorescence imaging of the excised organs (tumor, heart, liver, spleen, lung and kidney) at 3 h tumor injection of BODIPY-βgal. Note: fluorescence signals at 600 nm (rainbow scale) and 730 nm (yellow-red scale).

maximum level after 3 h post injection, while the 600 nm signal almost disappeared. To further confirm that the dual-channel fluorescent signal comes from the cleavage of BODIPY-βgal by β-gal in the tumor cells, we also recorded the *ex vivo* fluorescence images of the tumor cells and other normal organs after sacrificing the mice at 3 h post injection. Consistent with the *in vivo* results, only the tumor cells appeared fluorescent (Fig. 3e–h). These results confirm that the dual-channel NIR probe BODIPY-βgal has the capability to selectively detect and image β-gal *in vivo*.

In summary, we have developed a ratiometric and light-up NIR probe BODIPY-βgal, which is composed of monostyryl-substituted BODIPY-OH as a wavelength controllable fluorescent reporter with effective ICT properties, and a β-gal cleavable unit as an enzyme-specific trigger. There was a significant new enhanced emission peak at 730 nm, whereas the initial fluorescence at 575 nm of BODIPY-βgal was decreased in the presence of β-gal. Importantly, this probe was successfully applied for real-time trapping of intracellular endogenous β-gal distribution in overexpressed living SKOV-3 cells, as well as *in vivo* visualization of β-gal activity in a mice model. In light of its simplicity, sensitivity, and resistance to photobleaching, this enzyme-activatable ratiometric and light-up NIR fluorescent probe provides an accessible tool for *in vivo* targeted visualization and a therapeutic evaluation approach.

This work was supported by the NSFC/China (21622602, 21788102, 21421004, 21636002, 21878087 and 21908060), the National Key Research and Development Program (2017YFC-0906902), the Innovation Program of Shanghai Municipal Education Commission, the Scientific Committee of Shanghai (15XD1501400), the Shuguang Program (18SG27) and the China Postdoctoral Science Foundation (Grant 2019M651417). This study was performed in strict accordance with the NIH guidelines for the care and use of laboratory animals and was approved by the Institutional Animal Care and Use Committee of the National Tissue Engineering Center (Shanghai, China).

Conflicts of interest

There are no conflicts to declare.

Notes and references

1 C. Zhang, L. Yan, Z. Gu and Y. Zhao, *Chem. Sci.*, 2019, **10**, 6932–6943.
2 Y. Wang, K. Zhou, G. Huang, C. Hensley, X. Huang, X. Ma, T. Zhao, B. D. Sumer, R. J. DeBerardinis and J. Gao, *Nat. Mater.*, 2014, **13**, 204–212.
3 H. S. Jung, J. H. Lee, K. Kim, S. Koo, P. Verwilst, J. L. Sessler, C. Kang and J. S. Kim, *J. Am. Chem. Soc.*, 2017, **139**, 9972–9978.
4 X. Wu, W. Shi, X. Li and H. Ma, *Angew. Chem., Int. Ed.*, 2017, **56**, 15319–15323.
5 M. Li, J. Xia, R. Tian, J. Wang, J. Fan, J. Du, S. Long, X. Song, J. W. Foley and X. Peng, *J. Am. Chem. Soc.*, 2018, **140**, 14851–14859.
6 X. Liu, M. Xiang, Z. Tong, F. Luo, W. Chen, F. Liu, F. Wang, R. Q. Yu and J. H. Jiang, *Anal. Chem.*, 2018, **90**, 5534–5539.
7 J. Zhang, X. Chai, X. P. He, H. J. Kim, J. Yoon and H. Tian, *Chem. Soc. Rev.*, 2019, **48**, 683–722.
8 D. Asanuma, M. Sakabe, M. Kamiya, K. Yamamoto, J. Hiratake, M. Ogawa, N. Kosaka, P. L. Choyke, T. Nagano, H. Kobayashi and Y. Urano, *Nat. Commun.*, 2015, **6**, 6463.
9 H. M. Burke, T. Gunnlaugsson and E. M. Scanlan, *Chem. Commun.*, 2015, **51**, 10576–10588.
10 L. You, D. Zha and E. V. Anslyn, *Chem. Rev.*, 2015, **115**, 7840–7892.
11 X. Chen, F. Wang, J. Y. Hyun, T. Wei, J. Qiang, X. Ren, I. Shin and J. Yoon, *Chem. Soc. Rev.*, 2016, **45**, 2976–3016.
12 J. J. Kim, Y. A. Lee, D. Su, J. Lee, S. J. Park, B. Kim, J. H. J. Lee, X. Liu, S. S. Kim, M. A. Bae, J. S. Lee, S. C. Hong, L. Wang, A. Samanta, H. Y. Kwon, S. Y. Choi, J. Y. Kim, Y. H. Yu, H. H. Ha, Z. Wang, W. L. Tam, B. Lim, N. Y. Kang and Y. T. Chang, *J. Am. Chem. Soc.*, 2019, **141**, 14673–14686.
13 H. Y. Kwon, X. Liu, E. G. Choi, J. Y. Lee, S. Y. Choi, J. Y. Kim, L. Wang, S. J. Park, B. Kim, Y. A. Lee, J. J. Kim, N. Y. Kang and Y. T. Chang, *Angew. Chem., Int. Ed.*, 2019, **58**, 8426–8431.
14 Q. Qi, W. Chi, Y. Li, Q. Qiao, J. Chen, L. Miao, Y. Zhang, J. Li, W. Ji, T. Xu, X. Liu, J. Yoon and Z. Xu, *Chem. Sci.*, 2019, **10**, 4914–4922.
15 E. Calatrava-Perez, S. A. Bright, S. Achermann, C. Moylan, M. O. Senge, E. B. Veale, D. C. Williams, T. Gunnlaugsson and E. M. Scanlan, *Chem. Commun.*, 2016, **52**, 13086–13089.
16 G. Jiang, G. Zeng, W. Zhu, Y. Li, X. Dong, G. Zhang, X. Fan, J. Wang, Y. Wu and B. Z. Tang, *Chem. Commun.*, 2017, **53**, 4505–4508.
17 W. Chen, S. Xu, J. J. Day, D. Wang and M. Xian, *Angew. Chem., Int. Ed.*, 2017, **56**, 16611–16615.
18 Z. Guo, Y. Ma, Y. Liu, C. Yan, P. Shi, H. Tian and W.-H. Zhu, *Sci. China: Chem.*, 2018, **61**, 1293–1300.
19 D. Cheng, J. Peng, Y. Lv, D. Su, D. Liu, M. Chen, L. Yuan and X. Zhang, *J. Am. Chem. Soc.*, 2019, **141**, 6352–6361.
20 X. F. Wang, H. Xiao, P. Z. Chen, Q. Z. Yang, B. Chen, C. H. Tung, Y. Z. Chen and L. Z. Wu, *J. Am. Chem. Soc.*, 2019, **141**, 5045–5050.
21 Y. Zhang, H. Chen, D. Chen, D. Wu, X. Chen, S. H. Liu and J. Yin, *Org. Biomol. Chem.*, 2015, **13**, 9760–9766.
22 M. Cao, H. Chen, D. Chen, Z. Xu, S. H. Liu, X. Chen and J. Yin, *Chem. Commun.*, 2016, **52**, 721–724.
23 M. H. Lee, J. S. Kim and J. L. Sessler, *Chem. Soc. Rev.*, 2015, **44**, 4185–4191.
24 P. Zhang, Z.-Q. Guo, C.-X. Yan and W.-H. Zhu, *Chin. Chem. Lett.*, 2017, **28**, 1952–1956.
25 G. Xu, Q. Yan, X. Lv, Y. Zhu, K. Xin, B. Shi, R. Wang, J. Chen, W. Gao, P. Shi, C. Fan, C. Zhao and H. Tian, *Angew. Chem., Int. Ed.*, 2018, **57**, 3626–3630.
26 S. Long, Q. Qiao, L. Miao and Z. Xu, *Chin. Chem. Lett.*, 2019, **30**, 573–576.
27 R. Wang, K. Dong, G. Xu, B. Shi, T. Zhu, P. Shi, Z. Guo, W. H. Zhu and C. Zhao, *Chem. Sci.*, 2019, **10**, 2785–2790.
28 I. S. Turan, G. Gunaydin, S. Ayan and E. U. Akkaya, *Nat. Commun.*, 2018, **9**, 805.
29 X. X. Chen, L. Y. Niu, N. Shao and Q. Z. Yang, *Anal. Chem.*, 2019, **91**, 4301–4306.
30 M. Liu, S. Ma, M. She, J. Chen, Z. Wang, P. Liu, S. Zhang and J. Li, *Chin. Chem. Lett.*, 2019, DOI: 10.1016/j.cclet.2019.08.028.
31 J. S. Lee, N. Y. Kang, Y. K. Kim, A. Samanta, S. Feng, H. K. Kim, M. Vendrell, J. H. Park and Y. T. Chang, *J. Am. Chem. Soc.*, 2009, **131**, 10077–10082.
32 J. Cheng, B. Shao, S. Zhang, Y. Hu and X. Li, *RSC Adv.*, 2015, **5**, 65203–65207.
33 F. Deng, S. Long, Q. Qiao and Z. Xu, *Chem. Commun.*, 2018, **54**, 6157–6160.
34 E. J. Kim, R. Kumar, A. Sharma, B. Yoon, H. M. Kim, H. Lee, K. S. Hong and J. S. Kim, *Biomaterials*, 2017, **122**, 83–90.